Hindawi
Complexity
Volume 2020, Article ID 5859273, 16 pages
https://doi.org/10.1155/2020/5859273

Research Article

Secure Communication Scheme Based on a New 5D Multistable Four-Wing Memristive Hyperchaotic System with Disturbance Inputs

Fei Yu[1], **Zinan Zhang**[1], **Li Liu**[1], **Hui Shen**[1], **Yuanyuan Huang**[1], **Changqiong Shi**[1], **Shuo Cai**[1], **Yun Song**[1], **Sichun Du**[2] and **Quan Xu**[3]

[1]*School of Computer and Communication Engineering, Changsha University of Science and Technology, Changsha 410114, China*
[2]*College of Computer Science and Electronic Engineering, Hunan University, Changsha 410082, China*
[3]*School of Information Science and Engineering, Changzhou University, Changzhou 213164, China*

Correspondence should be addressed to Fei Yu; yufeiyfyf@csust.edu.cn and Yuanyuan Huang; snailhyy@126.com

Received 9 October 2019; Revised 12 November 2019; Accepted 22 November 2019; Published 10 January 2020

Guest Editor: Viet-Thanh Pham

By introducing a flux-controlled memristor model with absolute value function, a 5D multistable four-wing memristive hyperchaotic system (FWMHS) with linear equilibrium points is proposed in this paper. The dynamic characteristics of the system are studied in terms of equilibrium point, perpetual point, bifurcation diagram, Lyapunov exponential spectrum, phase portraits, and spectral entropy. This system is of the group of systems that have coexisting attractors. In addition, the circuit implementation scheme is also proposed. Then, a secure communication scheme based on the proposed 5D multistable FWMHS with disturbance inputs is designed. Based on parametric modulation theory and Lyapunov stability theory, synchronization and secure communication between the transmitter and receiver are realized and two message signals are recovered by a convenient robust high-order sliding mode adaptive controller. Through the proposed adaptive controller, the unknown parameters can be identified accurately, the gain of the receiver system can be adjusted continuously, and the disturbance inputs of the transmitter and receiver can be suppressed effectively. Thereafter, the convergence of the proposed scheme is proven by means of an appropriate Lyapunov functional and the effectiveness of the theoretical results is testified via numerical simulations.

1. Introduction

Chaotic signals are naturally invisible because of their non-periodic continuous bandwidth spectrum, similar noise, and extreme sensitivity to initial values. Therefore, in the past decade, chaos has attracted more and more scientists' interest and research in the fields of complex networks [1–3], electronic circuits [4–6], image encryption [7–9], synchronization [10–11], random number generator [12, 13], and secure communications [14–16]. In chaotic communication systems, how to generate chaotic signals suitable for modulation and spread spectrum has become an issue of concern [17, 18]. Several methods for generating complex chaotic signals are proposed, among which the generations of four-wing [19–21], multiwing [22–24], and multiscroll [25–29] chaotic attractors are the important achievements in recent years. Compared with chaotic systems, hyperchaotic systems have two or more positive Lyapunov exponents, and their motion orbits are separated in many directions, showing more complex dynamic behavior [30–34]. Complex hyperchaotic signals can improve the security of chaotic secure communication and chaotic information encryption, so hyperchaos will have a very broad application prospect in the field of information engineering.

Memristor has the advantages of nanometer size, automatic memory, and nonlinear characteristics. Compared with the traditional chaotic circuit system, a memristor chaotic circuit has more complex chaotic characteristics because the system is sensitive to circuit parameters and depends on the initial value of the memristor [35–39]. Chaotic signals generated by memristor chaotic systems have stronger pseudorandomness, which makes them have a broader application prospect in traditional chaotic applications.

Therefore, it is of great practical significance to design a chaotic system and circuit based on a memristor by combining the memristor with a nonlinear chaotic system. The generation of new multiwing hyperchaotic attractors based on memristors has become a research hotspot, and many such hyperchaotic systems have been introduced in recent years. In [39], by introducing a flux-controlled memristor into a multiwing system, no equilibrium hyperchaotic multiwing attractors are observed in the memristive system. A flux-controlled memristor with linear memductance is proposed in [40]; then, a new hyperchaotic system is presented by adding the proposed memristor into the Lorenz system, and the memristive system exhibits complex dynamic characteristics such as four-wing hyperchaotic attractors.

Multistability is one of the most important phenomena in dynamic systems [41–50], which occurs in many fields such as physics, biology, chemistry, economics, and electronics. Multistability allows flexibility of system performance without changing parameters, and appropriate control strategies can be used to induce switching behavior between different coexisting states [41]. For chaotic systems, hidden attractors [42–46] and infinite attractors [47–50] can exhibit multistability. For example, complex dynamic behaviors of coexisting attractors [51], transient chaos [52], and limit cycle [53] can be observed from hidden attractors. Recently, various multistable memristive hyperchaotic systems have been proposed in many literatures. In [52], by introducing a flux-controlled memristor model into an existing 5D hyperchaotic autonomous system, a 6D hyperchaotic autonomous system with hidden extreme multistability is proposed. Some attractive dynamics are observed like transient chaos, bursting, and offset boosting phenomenon. In [53], by utilizing a memristor to substitute a coupling resistor in the realization circuit of a 3D chaotic system having one saddle and two stable node-foci, a novel memristive hyperchaotic system with coexisting infinite hidden attractors is presented. The memristive system does not show any equilibrium but can exhibit hyperchaos, chaos, periodic dynamics, and transient hyperchaos.

With the application of network information technology, people attach great importance to the security and confidentiality of information [54–66]. Researchers are constantly looking for new methods of confidentiality [54–66]. Secure communication and chaotic encryption based on chaotic synchronization have become one of the research hotspots in the field of information security in recent years. In recent years, the secure communication scheme based on chaotic synchronization control has attracted extensive attention. People have made a thorough study on it and proposed various effective chaotic control methods, such as adaptive control [67–68], active control [69], linear feedback control [70, 71], and sliding mode control [72, 73]. In [69], the synchronization of 3D chaotic systems with the same structure is realized by using active control and adaptive control law. In the developed secure communication system, information signal sent over noisy channel is successfully retrieved at the receiver. In [72], a secure communication mechanism based on a four-wing 4D chaotic system is designed. Using high-order sliding mode control synchronization technology, parameter modulation method, and Lyapunov stability theory, two useful signals are encrypted and recovered and the external interference is suppressed.

Based on the above studies, a 5D multistable FWMHS is proposed based on the flux-controlled memristor model with absolute value function, from which the coexisting phenomenon of many hidden attractors are observed. Hyperchaos is exhibited with a line of equilibria. After that, circuitry implementation of the proposed system is investigated. Then, an adaptive asymptotic method is proposed to identify the 5D multistable FWMHS with several unknown parameters and to apply chaotic parameter modulation in secure communication. By this method, chaotic synchronization can be realized, unknown parameters can be identified, message signals can be recovered, and disturbance inputs can be suppressed simultaneously via a high-order sliding mode adaptive controller, whose adaptive parameters are adjusted according to the proposed adaptive algorithm. By using Lyapunov functional and Barbalat's lemma, the convergence of the proposed scheme is analyzed. Finally, two triangular wave signals are taken as examples for numerical simulation. The results show the effectiveness and feasibility of the proposed secure communication scheme.

2. New 5D Multistable FWMHS and Its Dynamics

2.1. System Description. A simple 5D chaotic oscillator with five parameters and five nonlinearities is proposed, and a flux-controlled memristor model with absolute value function is introduced to establish the mathematical model of the system:

$$\begin{cases} \dot{x}_1 = -ax_1 + x_2x_3, \\ \dot{x}_2 = bx_2 - x_1x_3, \\ \dot{x}_3 = x_1x_2 - cx_3 + dx_4W(x_5), \\ \dot{x}_4 = x_1x_2 - ex_4, \\ \dot{x}_5 = -x_3, \end{cases} \tag{1}$$

where a, b, c, d, and e are the parameters of the system and x_1, x_2, x_3, x_4, and x_5 are state variables. The memductance function $W(\psi) = 1 - \beta|\psi|$ [52], ψ and β being its flux variable and positive constant parameter, respectively. It is easy to see that system (1) is invariant under the transformation $(x_1, x_2, x_3, x_4, x_5) \longrightarrow (\pm x_1, \mp x_2, x_3, x_4, x_5)$. Thus, if $(x_1, x_2, x_3, x_4, x_5)$ is a solution for a specific set of parameters, then $(\pm x_1, \mp x_2, x_3, x_4, x_5)$ is also a solution for the same parameters set. So, the appearances of multiple coexisting symmetric attractors are expected in the new system.

When the parameters are chosen as $a = 10, b = 12$, $c = 30, d = 2, e = 3$, and $\beta = 0.2$, the Lyapunov exponents of system (1) are calculated as LE1 = 3.5610, LE2 = 0.3092, LE3 = 0, LE4 = −2.0660, and LE5 = −23.4708. It can be seen that there are two positive Lyapunov exponents which means system (1) can exhibit hyperchaotic dynamics. A typical four-wing hyperchaotic attractor from system (1) is shown in Figure 1, while the initial conditions are selected as $[0.1, 0.1, 0.1, 0.1, 0.1]$.

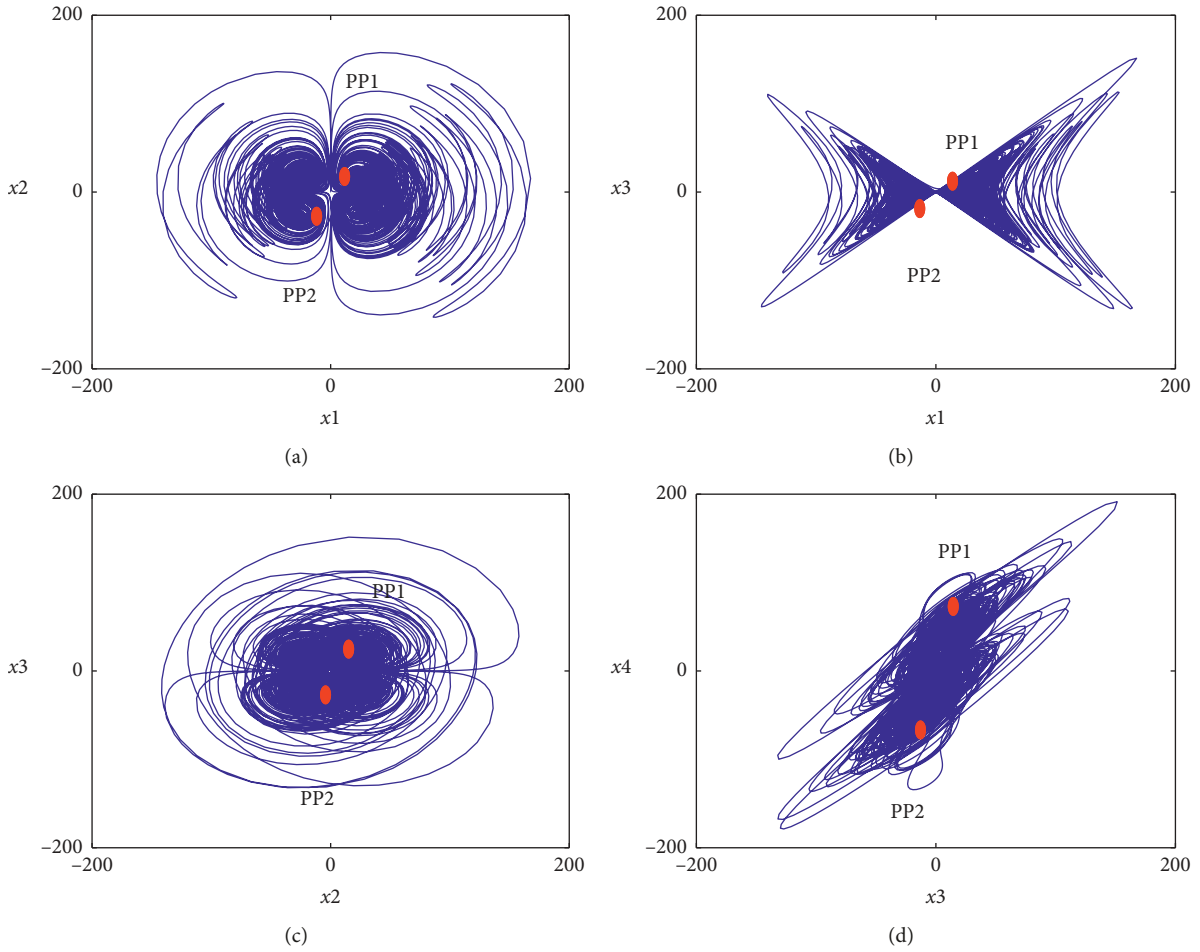

Figure 1: A typical four-wing hyperchaotic attractor of the 5D FWMHS (1) and perpetual points (red) in the (a) $x_1 - x_2$ plane, (b) $x_1 - x_3$ plane, (c) $x_2 - x_3$ plane, and (d) $x_3 - x_4$ plane.

2.2. Dissipativity. The volume contraction rate of system (1) is given by the following Lie derivatives:

$$\nabla V = \frac{\partial \dot{x}_1}{\partial x_1} + \frac{\partial \dot{x}_2}{\partial x_2} + \frac{\partial \dot{x}_3}{\partial x_3} + \frac{\partial \dot{x}_4}{\partial x_4} + \frac{\partial \dot{x}_5}{\partial x_5} = -a + b - c - e. \quad (2)$$

Equation (2) shows that divergence is negative when $-a + b - c - e < 0$. In this case, the set of system trajectories is ultimately limited to a specific zero volume limit set and the asymptotic motion of the new four-wing hyperchaotic system (1) falls on the attractor.

2.3. Equilibrium Points and Stability. Equilibrium points play an important role in the study of nonlinear systems because they allow the system response to be characterized as self-excited oscillation or hidden oscillation. These oscillations originate around the equilibrium point obtained from system (1), by setting the left-hand side to zero as follows:

$$\begin{cases} 0 = -ax_1 + x_2x_3, \\ 0 = bx_2 - x_1x_3, \\ 0 = x_1x_2 - cx_3 + dx_4W(x_5), \\ 0 = x_1x_2 - ex_4, \\ 0 = -x_3. \end{cases} \quad (3)$$

It can be seen that the equilibrium states of system (3) only depends on x_1, x_2, x_3, and x_4, but independent of x_5. System (3) has the abnormal characteristics of linear equilibrium in $(0, 0, 0, 0, x_5)$. Since x_5 in equilibrium can be any constant, assuming that l is a real constant, the equilibrium of system (3) can be described as follows:

$$O = \left\{(x_1, x_2, x_3, x_4, x_5) \,\middle|\, x_1 = x_2 = x_3 = x_4 = 0, x_5 = l\right\}. \quad (4)$$

The Jacobian matrix of system (3) at this line equilibrium is

$$J_O = \begin{bmatrix} -a & 0 & 0 & 0 & 0 \\ 0 & b & 0 & 0 & 0 \\ 0 & 0 & -c & d(1 - \beta|l|) & 0 \\ 0 & 0 & 0 & -e & 0 \\ 0 & 0 & 0 & -1 & 0 \end{bmatrix}. \quad (5)$$

According to Jacobian matrix (5), the characteristic equation of system (1) can be expressed as follows:

$$\lambda(\lambda + e)(\lambda + a)(\lambda - b)(\lambda + c) = 0. \quad (6)$$

Five eigenvalues of system (1) can be obtained from equation (6): $\lambda_1 = 0, \lambda_2 = -e, \lambda_3 = -a, \lambda_4 = b$, and $\lambda_5 = -c$. When $a = 10, b = 12, c = 30$, and $e = 3$, it is obvious that there are $\lambda_1 = 0, \lambda_{2,3,5} < 0$, and $\lambda_4 > 0$. Therefore, regardless of the parameter values, when system (1) has a line equilibrium, there is one zero eigenvalue, one positive eigenvalue, and three negative eigenvalues, so system (1) has unstable saddle points.

2.4. Perpetual Points. In this paper, we study the new kind of critical points proposed by Prasad in [74], which are called perpetual points. They are defined as points where the acceleration of the system becomes zero and the velocity remains nonzero. According to the number of zero derivatives, permanent points can belong to any regular point set except R^0. The various interesting properties and uses of these points can be found in [74–76]. According to the definition of perpetual points in [74], system (1) possesses two permanent points: PP1 = $(\sqrt{\text{bce}/(e+d)}, \sqrt{\text{ace}/(e+d)}, \sqrt{\text{ab}}, c(\sqrt{\text{ab}}/(e+d)), 0)$ and PP2 = $(-\sqrt{\text{bce}/(e+d)}, -\sqrt{\text{ace}/(e+d)}, -\sqrt{\text{ab}}, -c(\sqrt{\text{ab}}/(e+d)), 0)$. When $a = 10, b = 12, c = 30, d = 2$, and $e = 3$, the two permanent points are $(\pm 14.697, \pm 13.416, \pm 10.954, \pm 65.727, 0)$, which are shown in Figure 1, while perpetual points are denoted by red dots. We can see that the trajectories of the attractors pass through the perpetual points, so coexistence attractors can also be located using perpetual points.

2.5. Bifurcation Diagram and Lyapunov Exponent Spectrum. Bifurcation diagram and Lyapunov exponent spectrum are suitable tools for visualizing different scenes to chaos/hyperchaos in dynamic systems. When the system parameters change, this is achieved by the expression of the local maximum or minimum of the state variables. In order to study the dynamic behavior of the 5D FWMHS with parameters, we discuss the bifurcation diagram and Lyapunov exponent spectrum of the system with increasing parameter d by using Wolf's algorithm and maximum method, respectively. Figures 2 and 3 show the bifurcation diagram of the state $|X|$ and the corresponding Lyapunov exponents' spectrum with the range of the parameter d taken as $[0, 15]$, respectively, under the initial conditions of $[0.1, 0.1, 0.1, 0.1, 0.1]$. It can be seen that the bifurcation diagram is in good agreement with the Lyapunov exponent spectrum. When $0 \le d \le 7.52$, the system has two positive Lyapunov exponents and the system is in the hyperchaotic state; when $7.52 < d \le 10.1$, the system is in the periodic state; when $10.1 < d \le 15$, the system has one positive Lyapunov exponent, so the system is in the chaotic state.

2.6. The Complexity of Spectral Entropy. The complexity of spectral entropy reflects the disorder in the Fourier domain. We usually measure the complexity of a system by calculating its spectral entropy. The larger the spectral entropy is, the higher the complexity is, and vice versa

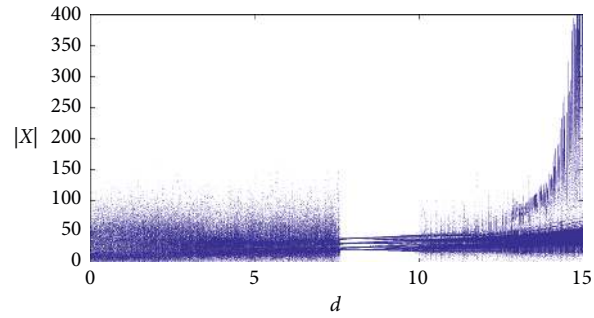

Figure 2: Bifurcation diagram for increasing parameter d.

[77–79]. In this part, the complexity of chaotic system (1) in the parameter range is analyzed by using spectral entropy complexity algorithm. Figure 4 is the complexity curve of the parameter $d \in [0, 12]$, which is very consistent with the Lyapunov exponents spectrum of system (1). When the parameter $d \in [0, 7.52]$, the Lyapunov exponents show that the system is hyperchaos. Similarly, Figure 4 also shows that the waveform changes steeply in this region, which means that the more complex the spectrum, the higher the complexity. When $d \in (7.52, 10.1]$, the waveform changes gently, so the spectrum is simple and the complexity is low; when $d \in (10.1, 12]$, the system is in the chaos state, and the spectral entropy complexity curve of the system changes greatly, so the complexity is very high.

2.7. Multistability Analysis. Multistability, the result of coexistence of many kinds of nonlinear attractors, is the inherent property of many nonlinear dynamic systems. In recent years, it has become a very important research topic and has attracted much attention [41–50]. Multistability is rich in the diversity of stable states of nonlinear dynamic systems, which makes the system flexible. In particular, when the number of coexisting attractors from a dynamic system tends to infinite, the coexistence of infinite attractors depending on the initial conditions of a state variable is called extreme multistability [80].

In order to investigate the possible multistability in this 5D FWMHS, we first consider random initial conditions while all the parameters are fixed. These coexisting attractors exist in different values of all parameters, and Figure 5 shows some symmetric coexisting attractors in state space of system (1) for different values of the parameter d. Figure 6 shows some coexisting multiwing attractors in state space of system (1) for different values of the parameter d with different initial conditions. As can be seen in Figure 6, the occurrence of chaos/hyperchaos, period, and quasi-period attractors coexist with each other for selected initial conditions.

3. Circuit Design

The above conclusions can be verified by the analog circuit. The analog circuit is a method that can really present the chaotic motion state, which is more convincing than

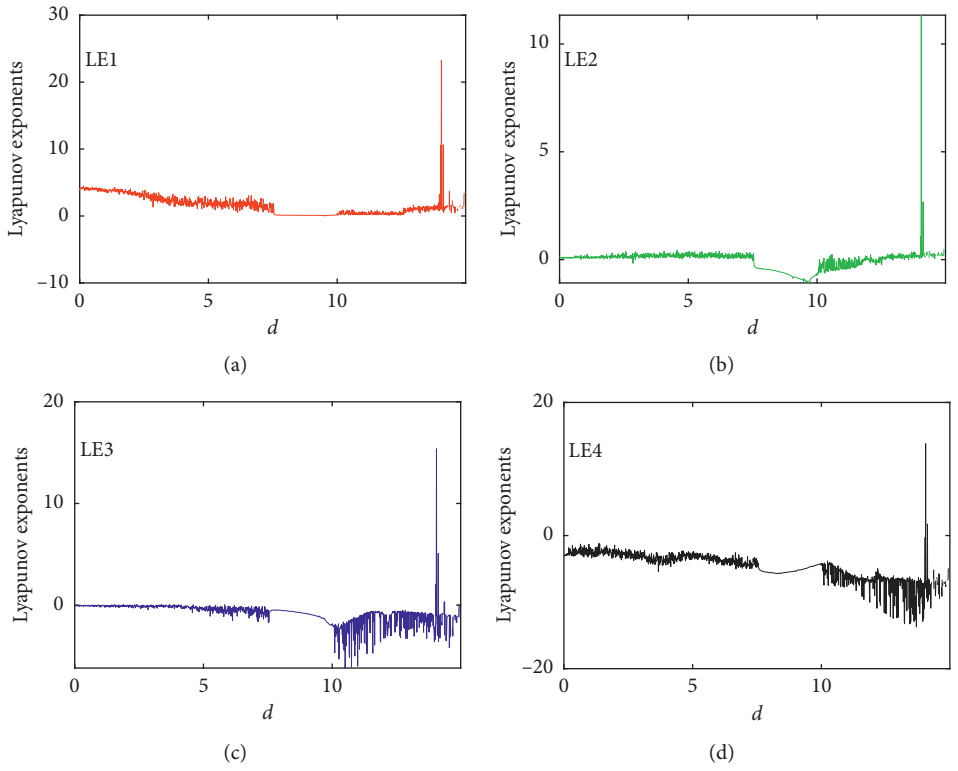

Figure 3: Lyapunov exponents' spectrum for increasing parameter d (the fifth LE is out of plot).

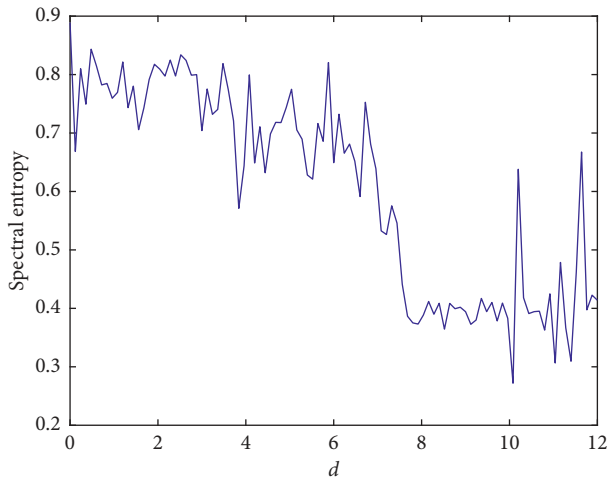

Figure 4: The complexity of spectral entropy for increasing parameter d.

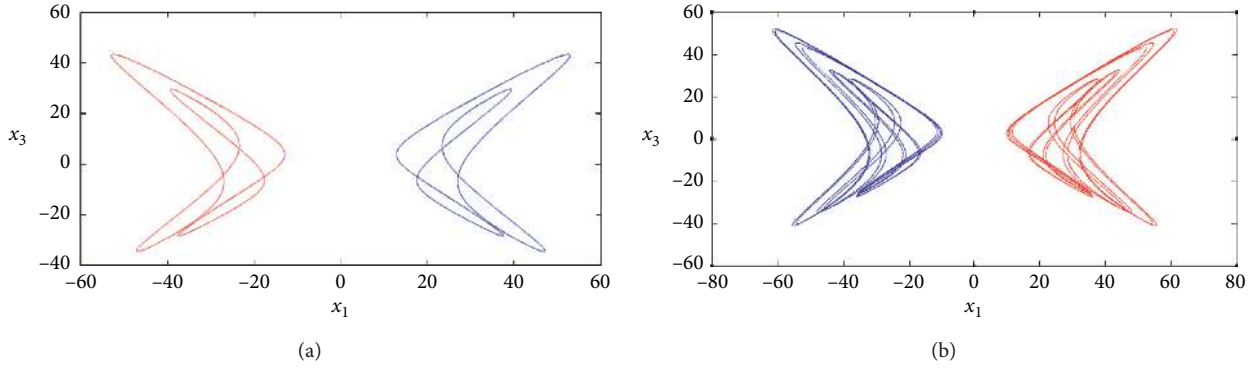

Figure 5: Continued.

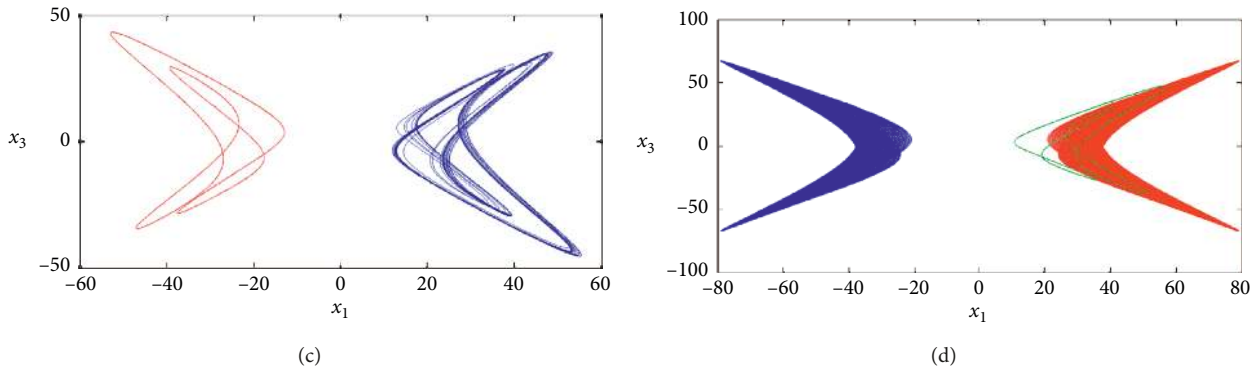

Figure 5: Symmetric coexisting attractors for parameters: (a) $d = 9$ and the initial conditions are $[0.1, \pm 0.1, 0.1, 0.1, 0.1]$ (red and blue), (b) $d = 12.5$ and the initial conditions are $[0.1, -0.1, 0.1, 0.1, 0.1]$ and $[-0.1, 0.1, 0.1, 0.1, 0.1]$ (red and blue), (c) $d = 9$ and the initial conditions are $[0.1, -0.1, 0.1, 0.1, 0.1]$ and $[2, 1, 1, 2, 2]$ (red and blue), and (d) $d = 11.9$ and the initial conditions are $[-0.1, 0.1, 0.1, 0.1, 0.1]$, $[0.1, -0.1, 0.1, 0.1, 0.1]$ and $[0.1, 0.1, 0.1, 0.1, 0.1]$ (blue, red, and green).

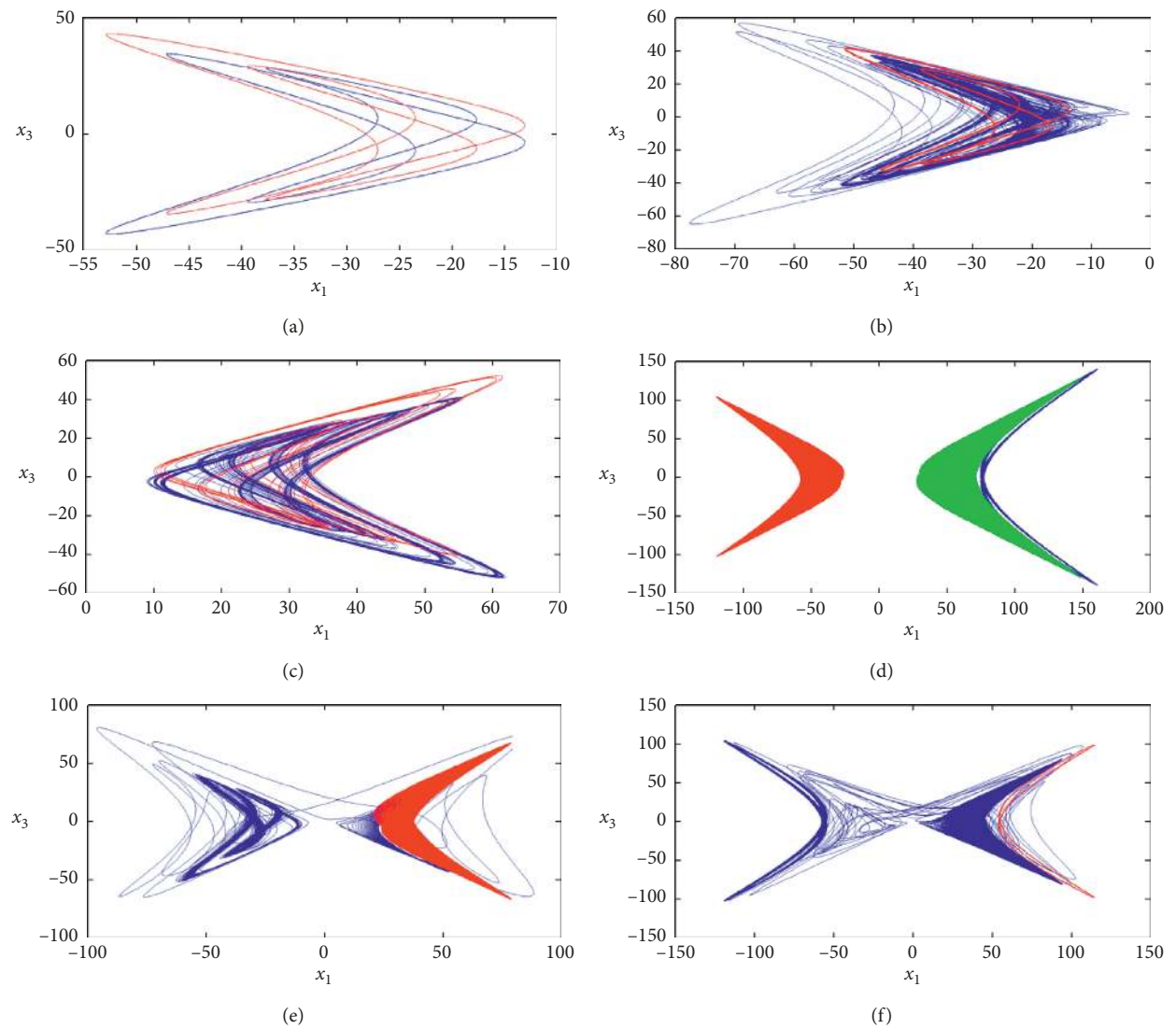

Figure 6: Coexisting multiwing attractors for parameters: (a) $d = 9$ and the initial conditions are $[0.1, -0.1, 0.1, 0.1, 0.1]$ and $[20, 1, 1, 2, 2]$ (red and blue), (b) $d = 8$ and the initial conditions are $[0.1, -0.1, 0.1, 0.1, 0.1]$ and $[20, 1, 1, 2, 2]$ (red and blue), (c) $d = 12.5$ and the initial conditions are $[0.1, -0.1, 0.1, 0.1, 0.1]$ and $[1, 0.1, 0.1, 0.1, 0.1]$ (red and blue), (d) $d = 13.5$ and the initial conditions are $[0.1, \pm 0.1, 0.1, 0.1, 0.1]$ and $[2, 1, 1, 2, 2]$ (blue, red, and green), (e) $d = 11.9$ and the initial conditions are $[0.1, -0.1, 0.1, 0.1, 0.1]$ and $[2, 1, 1, 2, 2]$ (red and blue), and (f) $d = 13$ and the initial conditions are $[0.1, 1, 0.1, 0.1, 0.1]$ and $[2, 1, 1, 2, 2]$ (red and blue).

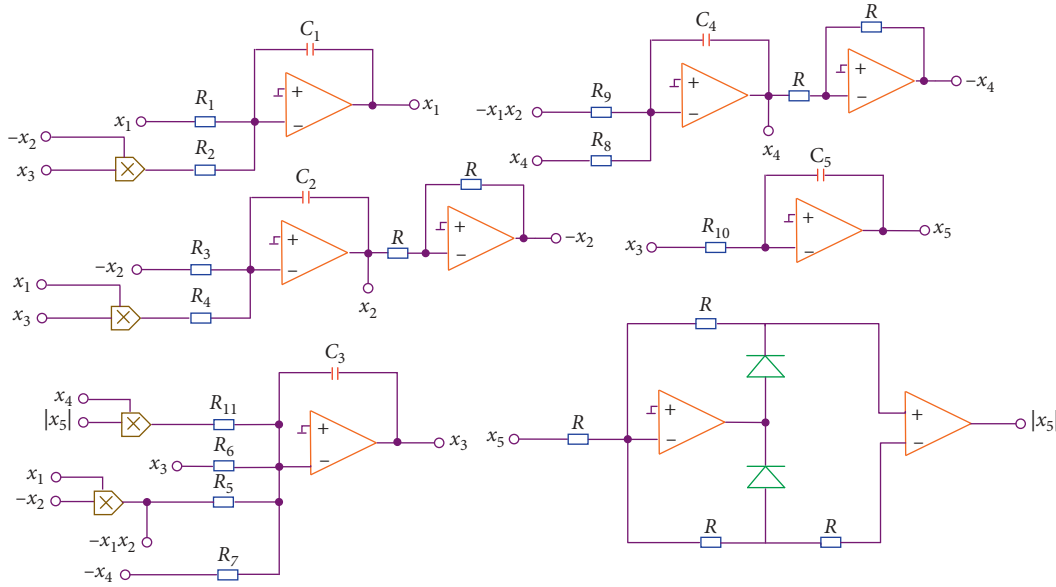

Figure 7: Hardware circuit implementation of the four-wing memristive hyperchaotic system (1).

numerical simulation. The operational amplifiers and multipliers are LF347 and AD633JN, respectively. Diode uses 1N1199C when all active components are powered with ±15 V. The schematic diagram of the circuit is designed with Multisim 14.0 software platform, as shown in Figure 7.

The simulation circuit designed according to the mathematical equation of each state of equation (1) is shown in Figure 7. In the simulation circuit, capacitors, resistors, analog multipliers, and integrated operational amplifiers are used (the memristor model has been split into two parts). According to the characteristics of the nonlinear circuit and the basic theory of the circuit, the mathematical equations of the states in the simulation circuit shown in Figure 7 are obtained as shown in the following equation:

$$\begin{cases} \dfrac{dx_1}{dt} = \dfrac{1}{R_1C_1}x_1 - \dfrac{1}{10R_2C_1}x_2x_3, \\ \dfrac{dx_2}{dt} = \dfrac{1}{R_3C_2}x_2 - \dfrac{1}{10R_4C_2}x_1x_3, \\ \dfrac{dx_3}{dt} = \dfrac{1}{10R_5C_3}x_1x_2 - \dfrac{1}{R_6C_3}x_3 + \dfrac{1}{R_7C_3}\left(1 - \dfrac{R_{12}}{R_{13}}|x_5|\right)x_4, \\ \dfrac{dx_4}{dt} = -\dfrac{1}{R_8C_4}x_4 + \dfrac{1}{10R_9C_4}x_1x_2, \\ \dfrac{dx_5}{dt} = -\dfrac{1}{R_{10}C_5}x_2. \end{cases} \tag{7}$$

According to the given parameters, the resistance value in (7) can be calculated as follows:

$$\begin{cases} \dfrac{R}{R_1} = 10, \quad R_1 = 10\,\text{k}\Omega, \\ \dfrac{R}{10R_2} = 1, \quad R_2 = 10\,\text{k}\Omega, \\ \dfrac{R}{R_3} = 12, \quad R_3 = 8.33\,\text{k}\Omega, \\ \dfrac{R}{10R_4} = 1, \quad R_4 = 10\,\text{k}\Omega, \\ \dfrac{R}{10R_5} = 1, \quad R_5 = 10\,\text{k}\Omega, \\ \dfrac{R}{R_6} = 30, \quad R_6 = 3.33\,\text{k}\Omega, \\ \dfrac{R}{R_7} = 2, \quad R_7 = 50\,\text{k}\Omega, \\ \dfrac{R}{R_8} = 3, \quad R_8 = 33.33\,\text{k}\Omega, \\ \dfrac{R}{10R_9} = 1, \quad R_9 = 10\,\text{k}\Omega, \\ \dfrac{R}{R_{10}} = 1, \quad R_{10} = 100\,\text{k}\Omega. \end{cases} \tag{8}$$

The other parameters of each component in the circuit are set as follows: $R = 100\,\text{k}\Omega$ and $C_1 = C_2 = C_3 = C_4 = 0.01\,\mu\text{F}$. Under the above parameters setting conditions, the hyperchaotic phase portraits are obtained, as shown in Figure 8(a)–8(d), respectively. From these diagrams, it can be seen that the circuit implementation results are basically consistent with the numerical simulation results.

4. Secure Communication Scheme Based on the New 5D Multistable FWMHS

In this section, based on the proposed 5D multistable FWMHS, a chaotic secure communication scheme with two inputs and two outputs is proposed. By using high-order sliding mode control synchronization technology, parameter modulation method, and Lyapunov stability theory, the encryption and recovery of two message signals are realized, the gain of the receiver can be continuously adjusted, the unknown parameters can be accurately identified, and the disturbance inputs can be suppressed simultaneously.

4.1. Higher-Order Sliding Mode Control Theory. The sliding order r of the traditional sliding mode (r refers to the number of continuous full derivatives of the sliding mode variable s which are zero on the sliding mode surface $s = 0$) is 1. Because $s = 0$ on the sliding mode surface, s is discontinuous, the traditional sliding mode is also called the first-order sliding mode. Traditional sliding mode control is essentially a discontinuous control input acting on the first derivative of the sliding mode, which makes the traditional sliding mode control have discontinuous and serious chattering problems. In order to restrain such problems, the theory of high-order sliding mode control is proposed. In the sense of Filippov, high-order sliding mode is actually a kind of motion on a special type of integral manifold of a discontinuous dynamic system [81]. It can be characterized by the convergence of switching function $s(x)$ and derivatives up to a certain order to zero. The order sliding set of sliding surface $s = 0$ is described as follows:

$$s = \dot{s} = \ddot{s} = \cdots = s^{(r-1)} = 0. \tag{9}$$

When the r-order sliding set (9) is nonempty and assumes that it is a local integral set in the sense of Filippov, the related motion satisfying the above formula is called "r-order sliding mode," with respect to the sliding surface $s = 0$. At present, there is a popular design method for high-order sliding mode variable structure control, i.e., gain-adjustable switching control. Its structure is as follows:

$$u = k\,\text{sgn}(s(x))s^r(x), \tag{10}$$

where the constant k is the control gain and can be adjusted. It can be seen that the high-order sliding mode control is to apply discontinuous control inputs to the high-order derivatives of the sliding mode, which can not only greatly weaken the chattering during system switching but also realize the high-order dynamic characteristics of the system [82]. Therefore, the high-order sliding mode maintains the advantages of the traditional sliding mode, suppresses the chattering, eliminates the restriction of relative order, and improves the control accuracy.

4.2. Some Definitions and Assumptions. Definition 1. Consider the following form of smooth nonlinear chaotic systems:

$$\begin{aligned} \dot{X} &= f(X, Q), \\ \dot{Y} &= h(X), \end{aligned} \tag{11}$$

where $X = (x_1, x_2, \ldots, x_n)^T \subset R^n$ is the state variable, $Y = (x_1, x_2, \ldots, x_m)^T \subset R^m$ is the output state variable, and $m \le n$. $f(\circ)$ and $h(\circ)$ are smooth nonlinear functions and $Q \subset R^l$ are state vectors satisfying $l \le n$. Let $\alpha^{(j)}$ be the reciprocal of j times of vector α. If X can be uniquely expressed by equation (12), we think that the state variable X can be observed by the algebraic method:

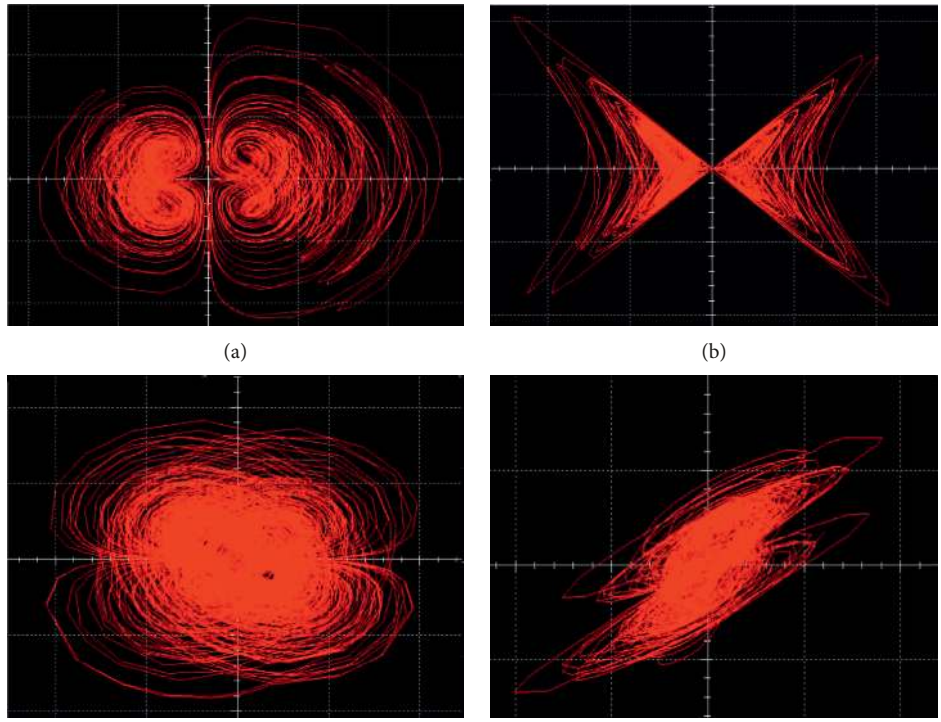

FIGURE 8: Four-wing memristive hyperchaotic phase portraits obtained by Multisim simulations in the (a) $x_1 - x_2$ plane, (b) $x_1 - x_3$ plane, (c) $x_2 - x_3$ plane, and (d) $x_3 - x_4$ plane.

$$X = \psi\left(\alpha, \alpha^{(1)}, \ldots, \alpha^{(j)}\right)^T, \tag{12}$$

where j is an integer and ψ is a smooth function.

Definition 2. Under the same conditions as Definition 1, when Q satisfies the following relationship:

$$\varphi_1\left(\alpha, \alpha^{(1)}, \ldots, \alpha^{(j)}\right) = \varphi_2\left(\alpha, \alpha^{(1)}, \ldots, \alpha^{(j)}\right)Q, \tag{13}$$

where $\varphi_1(\circ)$ and $\varphi_2(\circ)$ are smooth matrices of $n \times 1$ and $n \times n$, respectively, Q is considered to be observable with the algebraic method for output vector matrix α.

Assumption 1. The 5D multistable FWMHS (1) proposed above is selected as the transceiver system of the communication scheme. It is clear from Figures 1 and 2 that the five state variables of the system oscillate within a certain range. In fact, for most of the initial conditions and system parameters, the five state variables of system (1) are bounded in most cases.

Assumption 2. It is assumed that both transmitter and receiver systems of secure communication mechanism are subject to disturbance inputs of d_{1i}, $i = 1, 2, 3, 4, 5$ and d_{2i}, $i = 1, 2, 3, 4, 5$, respectively, and are bounded and satisfy $|d_{1i}| \le \rho_{1i}$, $i = 1, 2, 3, 4, 5$ and $|d_{2i}| \le \rho_{2i}$, $i = 1, 2, 3, 4, 5$, of which ρ_{2i}, ρ_{1i} are known positive constants and satisfy $\rho_{2i} \ge \rho_{1i}$.

Now, we rewrite the second difference equation of system (1) as follows:

$$x_3 = \frac{bx_2 - \dot{x}_2}{x_1}, \tag{14}$$

then equation (14) is substituted into the first equation of system (1) to obtain

$$x_1\dot{x}_1 + x_2\dot{x}_2 = bx_2^2 - ax_1^2. \tag{15}$$

According to Definitions 1 and 2, it is obvious that system (1) is observable by the algebraic method with respect to two outputs x_1 and x_2. According to equation (15), it is further shown that the state parameter vector $Q = [a, b]^T$ of system (1) can be observed algebraically with respect to the two outputs x_1 and x_2. Therefore, invalid states x_3, x_4, and x_5 and parameter vector Q can be recovered by the two output variables at the same time.

4.3. Transceiver Design. At the transmitter, we choose the 5D multistable FWMHS (1) as the drive system. The algebraic equation with some uncertain parameters and disturbance inputs is described as follows:

$$\begin{cases} \dot{x}_1 = -a(t)x_1 + x_2x_3 + d_{11}, \\ \dot{x}_2 = b(t)x_2 - x_1x_3 + d_{12}, \\ \dot{x}_3 = x_1x_2 - 30x_3 + 2x_4\left(1 - 0.2\left|x_5\right|\right) + d_{13}, \\ \dot{x}_4 = x_1x_2 - 3x_4 + d_{14}, \\ \dot{x}_5 = -x_3 + d_{15}, \end{cases} \tag{16}$$

where x_1, x_2, x_3, x_4, and x_5 are the state variables of the 5D multistable FWMHS, and the uncertain parameters are defined as follows:

$$a(t) = a + s_a(t), b(t) = b + s_b(t), \tag{17}$$

where $s_a(t)$ and $s_b(t)$ are two useful message signals, and the state parameter vector is $Q = [a, b]^T$. d_{1i}, $i = 1, 2, 3, 4, 5$, are disturbance inputs and satisfy Assumption 2.

At the receiver, we define the 5D multistable FWMHS (1) with partial uncertainties and disturbance inputs as a response system. The response system has two effective output variables x_1 and x_2, whose algebraic equation is described as follows:

$$\begin{cases} \dot{x}_6 = -\widehat{a}(t)x_1 + x_2x_8 + d_{21} + u_1, \\ \dot{x}_7 = \widehat{b}(t)x_2 - x_1x_8 + d_{22} + u_2, \\ \dot{x}_8 = x_1x_2 - 30x_8 + 2x_9\left(1 - 0.2\left|x_{10}\right|\right) + d_{23} + u_3, \\ \dot{x}_9 = x_1x_2 - 3x_9 + d_{24} + u_4, \\ \dot{x}_{10} = -x_8 + d_{25} + u_5, \end{cases} \tag{18}$$

where x_6, x_7, x_8, x_9, and x_{10} are the state variables of the system, and the uncertain parameters are defined as follows:

$$\widehat{a}(t) = \widehat{a} + \widehat{s}_a(t), \widehat{b}(t) = \widehat{b} + \widehat{s}_b(t), \tag{19}$$

where $\widehat{s}_a(t)$ and $\widehat{s}_b(t)$ are two useful message signals after decryption. d_{2i}, $i = 1, 2, 3, 4, 5$, are disturbance inputs and satisfy Assumption 2, $U = [u_1, u_2, u_3, u_4, u_5]^T$ are controllers, and $\widehat{Q} = [\widehat{a}, \widehat{b}]^T$. Figure 9 shows the proposed secure communication scheme based on two-input two-output with partial uncertainties and disturbance inputs.

4.4. Error Dynamics System Design. By subtracting system (16) from system (18), the following error dynamics system is obtained:

$$\dot{e} = \begin{bmatrix} \dot{e}_1 \\ \dot{e}_2 \\ \dot{e}_3 \\ \dot{e}_4 \\ \dot{e}_5 \end{bmatrix} = \begin{bmatrix} -\widetilde{a}x_1 - \widetilde{s}_a(t)x_1 + x_2e_3 + d_{11} - d_{21} - u_1 \\ \widetilde{b}x_2 + \widetilde{s}_b(t)x_2 - x_1e_3 + d_{12} - d_{22} - u_2 \\ -30e_3 + 2e_4 - 0.4\left(x_4\left|x_5\right| - x_9\left|x_{10}\right|\right) + d_{13} - d_{23} - u_3 \\ -3e_w + d_{14} - d_{24} - u_4 \\ -e_3 + d_{15} - d_{25} - u_5 \end{bmatrix}, \tag{20}$$

where

$$\begin{aligned} e &= \begin{bmatrix} e_1 \\ e_2 \\ e_3 \\ e_4 \\ e_5 \end{bmatrix} = \begin{bmatrix} x_1 - x_6 \\ x_2 - x_7 \\ x_3 - x_8 \\ x_4 - x_9 \\ x_5 - x_{10} \end{bmatrix}, \\ Q &= \begin{bmatrix} a \\ b \end{bmatrix}, \\ \widetilde{Q} &= \begin{bmatrix} \widetilde{a} \\ \widetilde{b} \end{bmatrix} = \begin{bmatrix} a - \widehat{a} \\ b - \widehat{b} \end{bmatrix}, \\ s(t) &= \begin{bmatrix} s_a(t) \\ s_b(t) \end{bmatrix}, \\ \widetilde{s}(t) &= \begin{bmatrix} \widetilde{s}_a(t) \\ \widetilde{s}_b(t) \end{bmatrix} = \begin{bmatrix} s_a(t) - \widehat{s}_a(t) \\ s_b(t) - \widehat{s}_b(t) \end{bmatrix}. \end{aligned} \tag{21}$$

It can be seen that the synchronization between system (16) and system (18) can be achieved as long as the appropriate controller $U = [u_1, u_2, u_3, u_4, u_5]^T$ and the corresponding parameter identification law are designed to make the error system approach zero gradually.

4.5. High-Order Sliding Mode Controller Design. Based on the idea of high-order sliding mode control proposed in the previous section, we present the following corresponding theory.

Theorem 1. *If the following high-order sliding mode adaptive controller is designed,*

$$U = \begin{bmatrix} u_1 \\ u_2 \\ u_3 \\ u_4 \\ u_5 \end{bmatrix} = \begin{bmatrix} k_1\mathrm{sign}(e_1)e_1^{\lambda} + \rho_{11}\mathrm{sign}(e_1) - \rho_{21}\mathrm{sign}(e_1) \\ k_2\mathrm{sign}(e_2)e_2^{\lambda} + \rho_{12}\mathrm{sign}(e_2) - \rho_{22}\mathrm{sign}(e_2) \\ x_2e_1 - x_1e_2 - 30e_3 - 0.4\left(x_4\left|x_5\right| - x_9\left|x_{10}\right|\right) + \rho_{13}\mathrm{sign}(e_3) - \rho_{23}\mathrm{sign}(e_3) \\ 2e_3 - 3e_4 + \rho_{14}\mathrm{sign}(e_4) - \rho_{24}\mathrm{sign}(e_4) \\ -e_3 + \rho_{15}\mathrm{sign}(e_5) - \rho_{25}\mathrm{sign}(e_5) \end{bmatrix}, \tag{22}$$

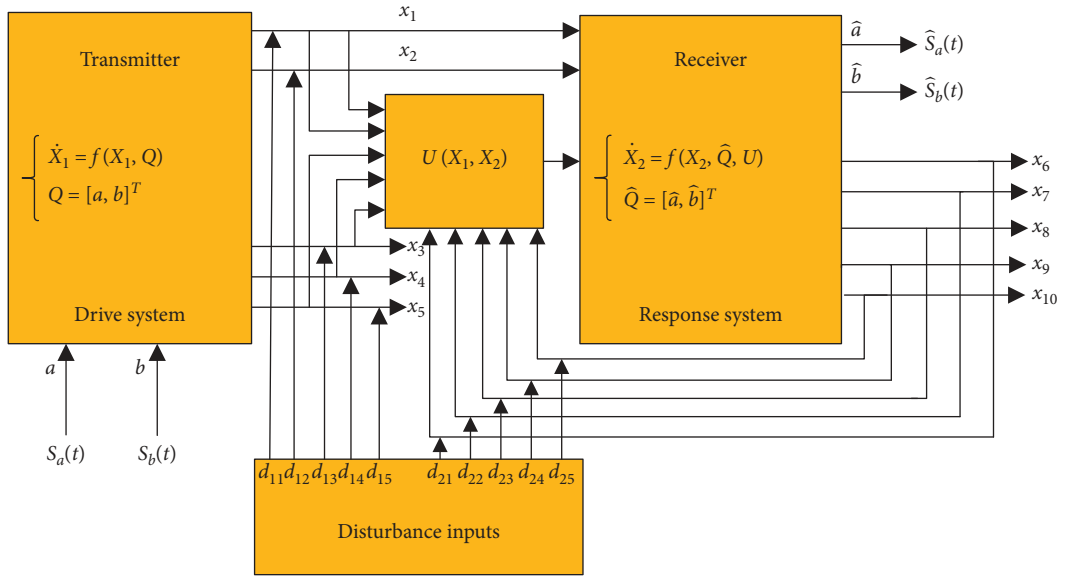

Figure 9: Secure communication scheme based on two-input and two-output with partial uncertainty parameters and disturbance inputs.

where $k = [k_1, k_2]^T$ is the controller gain, $\lambda \in Z^+, \lambda > 1$, and sign$(\circ)$ is symbolic function. The adaptive parameter identification law and the useful message signal law are designed as follows:

$$\dot{\hat{Q}} = \begin{bmatrix} \dot{\hat{a}} \\ \dot{\hat{b}} \end{bmatrix} = \begin{bmatrix} -x_1 e_1 \\ x_2 e_2 \end{bmatrix},$$
$$\dot{\hat{s}}(t) = \begin{bmatrix} \dot{\hat{s}}_a(t) \\ \dot{\hat{s}}_b(t) \end{bmatrix} = \begin{bmatrix} -x_1 e_1 \\ x_2 e_2 \end{bmatrix}, \tag{23}$$

where $\dot{\hat{a}}$ and $\dot{\hat{b}}$ are the estimates of unknown parameters and a and b are useful message signals for decryption. The response system (18) and the drive system (16) can be synchronized globally and asymptotically with disturbance inputs, any normal number k_1 and k_2, and any positive integer λ. By modulation laws (17), (19), and (22), the receiver system (18) can accurately recover useful message signals $s_a(t)$ and $s_b(t)$, respectively.

Proof. Consider the following Lyapunov function:

$$V(t) = \frac{1}{2}\left[e^T e + \tilde{Q}^T \tilde{Q} + \tilde{s}(t)^T \tilde{s}(t)\right]. \tag{24}$$

By calculating the derivative of $V(t)$ along the trajectories of the error system (19) and using equations (21) and (22), we can obtain

$$\begin{aligned}
\dot{V}(t) &= e_1\dot{e}_1 + e_2\dot{e}_2 + e_3\dot{e}_3 + e_4\dot{e}_4 + e_5\dot{e}_5 + \tilde{a}\dot{\tilde{a}} + \tilde{b}\dot{\tilde{b}} + \tilde{s}_a(t)\dot{\tilde{s}}_a(t) + \tilde{s}_b(t)\dot{\tilde{s}}_b(t) \\
&= -e_1\tilde{a}x_1 - e_1\tilde{s}_a(t)x_1 + e_1x_2e_3 + e_1d_{11} - e_1d_{21} - e_1k_1\text{sign}(e_1)e_1^\lambda - \rho_{11}e_1\text{sign}(e_1) \\
&\quad + \rho_{21}e_1\text{sign}(e_1) + \rho_{21}e_1\text{sign}(e_1) + e_2\tilde{b}x_2 + e_2\tilde{s}_b(t)x_2 - e_2x_1e_3 + e_2d_{12} - e_2d_{22} - e_2k_2\text{sign}(e_2)e_2^\lambda \\
&\quad - p_{12}e_2\text{sign}(e_2) + p_{22}e_2\text{sign}(e_2) - 30e_3^2 + 2e_3e_4 - 0.4e_4\left(x_4|x_5| - x_9|x_{10}|\right) + e_3d_{13} - e_3d_{13} - e_3d_{23} \\
&\quad - e_3x_2e_1 + x_1e_3e_2 + 30e_3^2 + 0.4e_4\left(x_4|x_5| - x_9|x_{10}|\right) - p_{13}e_3\text{sign}(e_3) + p_{23}e_3\text{sign}(e_3) + p_{23}e_3\text{sign}(e_3) - 3e_4^2 \\
&\quad + e_4d_{14} - e_4d_{24} - 2e_4e_3 + 3e_3^2 - p_{14}e_4\text{sign}(e_4) + p_{24}e_4\text{sign}(e_4) - e_3e_5 + e_5d_{15} - e_5d_{25} + e_3e_5 \\
&\quad - p_{15}e_5\text{sign}(e_5) + p_{25}e_5\text{sign}(e_5) + \tilde{a}x_1e_1 - \tilde{b}x_2e_2 + x_1e_1\tilde{s}_a(t) - x_2e_2\tilde{s}_b(t) \\
&= -k_1e_1\text{sign}(e_1)e_1^\lambda - k_2e_2\text{sign}(e_2)e_2^\lambda + e_1d_{11} - p_{11}e_1\text{sign}(e_1) - [e_1d_{21} - p_{21}e_1\text{sign}(e_1)] \\
&\quad + e_2d_{12} - p_{12}e_2\text{sign}(e_2) - [e_2d_{22} - p_{22}e_2\text{sign}(e_2)] + e_3d_{13} - p_{13}e_3\text{sign}(e_3) - [e_3d_{23} - p_{23}e_3\text{sign}(e_3)] \\
&\quad + e_4d_{14} - p_{14}e_4\text{sign}(e_4) - [e_4d_{24} - p_{24}e_4\text{sign}(e_4)] + e_5d_{15} - p_{15}e_5\text{sign}(e_5) \\
&\quad - [e_5d_{25} - p_{25}e_5\text{sign}(e_5)].
\end{aligned} \tag{25}$$

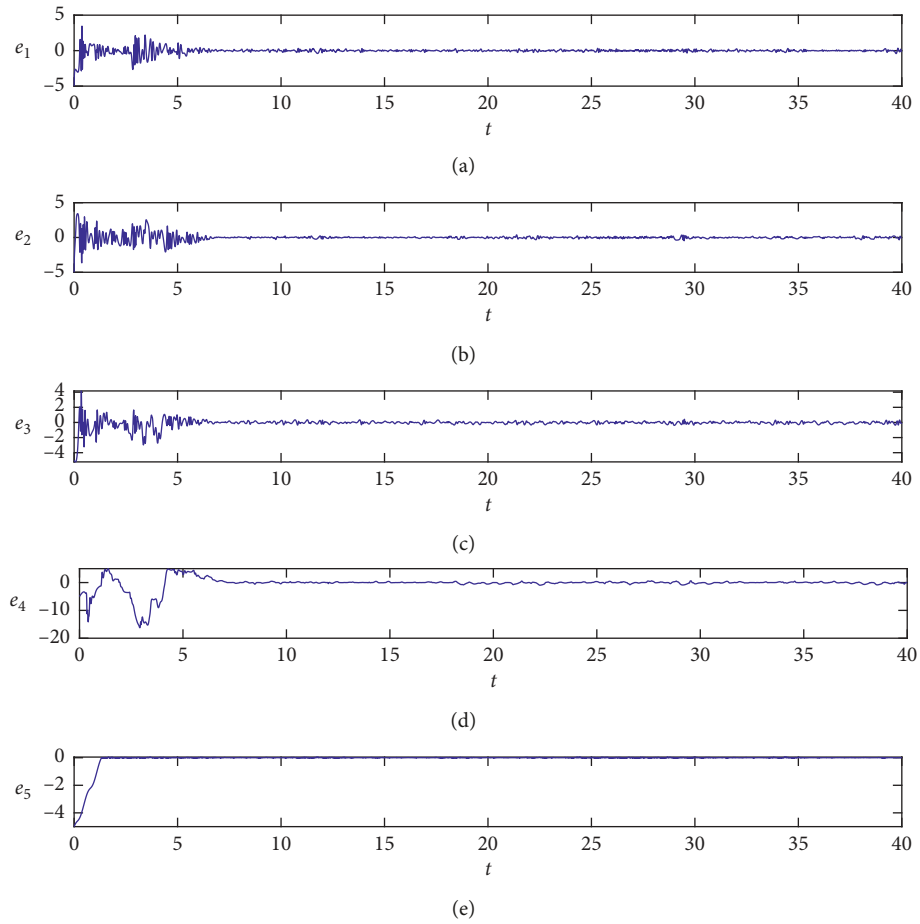

Figure 10: The trajectories of the synchronization errors e_1, e_2, e_3, e_4, and e_5.

When

$$\begin{cases} \psi_{1i} = e_i d_{1i} - \rho_{1i} e_i \operatorname{sign}(e_i), \\ \psi_{2i} = e_i d_{2i} - \rho_{2i} e_i \operatorname{sign}(e_i), \end{cases} \tag{26}$$

where ψ_{1i}, ψ_{2i}, $(i = 1, 2, 3, 4, 5) \in R$ are the compensators for eliminating disturbance inputs. According to the definitions and assumptions of d_{1i} and d_{2i} and ρ_{1i} and ρ_{2i}, $\psi_{1i} \le \psi_{2i}$ can be guaranteed, so (24) can be changed to

$$\begin{aligned} \dot{V}(t) &= -\left[k_1 e_1 \operatorname{sign}(e_1) e_1^{\lambda} + k_2 e_2 \operatorname{sign}(e_2) e_2^{\lambda}\right] + \sum_{i=1}^{4} (\psi_{1i} - \psi_{2i}) \\ &\le -\left[k_1 e_2 \operatorname{sign}(e_2) e_2^{\lambda} + k_2 e_2 \operatorname{sign}(e_2) e_2^{\lambda}\right] \\ &= -\left(k_1 |e_1| e_1^{\lambda} + k_2 |e_2| e_2^{\lambda}\right). \end{aligned} \tag{27}$$

So, $\dot{V}(t)$ is negative definite. In fact, because of $\dot{V}(t) < 0$, there are $e_1, e_2 \in L_{¥}$. The error equation (19) shows that $\dot{e}_1, \dot{e}_2 \in L_{¥}$. Integrating both sides of equation (27), it can be obtain:

$$\int_0^t \left(k_1 \left| e_1(t) \right| e_1^{\lambda}(t) + k_2 \left| e_2(t) \right| e_2^{\lambda}(t)\right) \mathrm{d}t \le V(0). \tag{28}$$

According to Barbalat's lemma, when $t \longrightarrow ¥$, there are $\dot{e} \longrightarrow ¥$. Therefore, the response system (18) with disturbance inputs and the drive system (16) with disturbance inputs achieve global asymptotic synchronization.

As shown in Figure 2, the state variables x_1 and x_2 oscillate aperiodically around the zero. From the above discussion, we can conclude that $\dot{e}$ is bounded, which means that e is continuous. According to Barbalat's lemma, when $t \longrightarrow ¥$, there are $\dot{e} \longrightarrow ¥$. By differentiating equation (19), we also get that ës is bounded, and when $t \longrightarrow ¥$, there is $\ddot{e} \longrightarrow ¥$. Since when $t \longrightarrow ¥$, $V(t)$ is convergent, it is obtained that when $t \longrightarrow ¥$, two uncertain parameter errors $\tilde{Q}$ and two useful message signal errors $\tilde{s}(t)$ are convergent. From equation (22), when $t \longrightarrow ¥$, $\tilde{Q}$s and $\dot{\tilde{s}}(t)$ converge to zero. Therefore, the uncertain parameters $a(t)$ and $b(t)$ at the receiver can be identified and the useful message signals $s_a(t)$ and $s_b(t)$ can be accurately recovered at the same time.

4.6. Numerical Simulations. In this section, the fourth-order Runge–Kutta method is used to simulate and verify the theoretical analysis with the step size 0.001. At the transmitter, the uncertain parameters of the system are selected as $a = 10$ and $b = 12$ and the initial conditions of the system are set to $x_1(0) = 1, x_2(0) = 2, x_3(0) = 3, x_4(0) = 4$, and $x_5(0) = 5$. At the receiver side, the initial conditions of the system are set to $x_6(0) = 6, x_7(0) = 7, x_8(0) = 8, x_9(0) = 9$, and

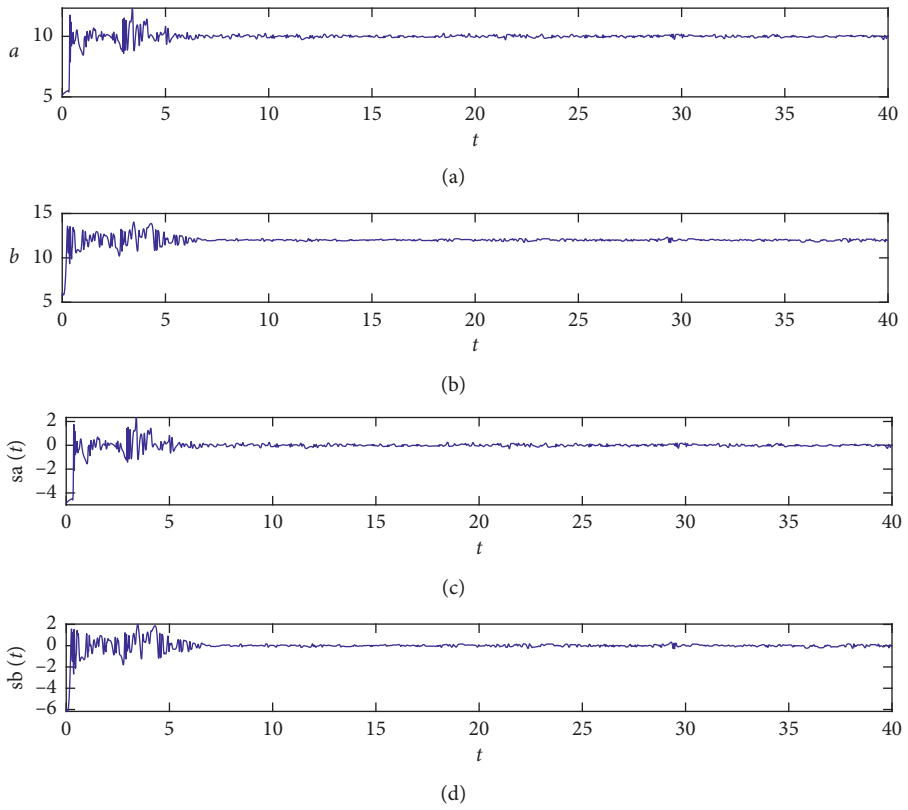

Figure 11: Estimation of uncertain parameters (a) and (b) and the recovered signal errors (c) and (d).

$x_{10}(0) = 10$. The initial conditions of uncertain parameters and useful message signals are set to $\widehat{Q}(0) = [\widehat{a}(0), \widehat{b}(0)]^T = [0.1, 0.1]^T$ and $\widehat{s}(0) = [\widehat{s}_a(0), \widehat{s}_b \quad (0)]^T = [0.1, 0.1]^T$, respectively. The disturbance inputs are set as follows:

$$\begin{cases} [d_{11}, d_{12}, d_{13}, d_{14}, d_{15}]^T = [-0.3\cos(20t), 0.2\sin(10t), 0.2\sin(10t), 0.2\cos(20t), 0.2\cos(20t)]^T, \\ [d_{21}, d_{22}, d_{23}, d_{24}, d_{25}]^T = [4\sin(20t), -3\cos(10t), 3\sin(20t), 2\sin(10t), 2\sin(10t)]^T. \end{cases} \tag{29}$$

Assuming that the useful message signals $s_a(t)$ and $s_b(t)$ are triangular function signals, and the frequencies of both triangular function signals are 90 Hz, we have

$$\begin{cases} s_a(t) = 0.6\sin(180\pi t), \\ s_b(t) = 0.5\cos(180\pi t). \end{cases} \tag{30}$$

At the same time, the gains of the receiver system are chosen as $k = [k_1, k_2]^T = [0.6, 0.8]^T$ and sliding order $\lambda = 4$. Figure 10 shows the synchronization error of the response system (18) and the drive system (16), indicating that the error tends to zero rapidly and gradually with time. Figures 11(a) and 11(b) show that when $t \longrightarrow ¥$, the estimated values of unknown parameters $\widehat{a}(t)$ and $\widehat{b}(t)$ gradually tend to $a = 10$ and $b = 12$ over time, respectively. As shown in Figures 11(c) and 11(d), it is easy to see that both useful message signals $s_a(t)$ and $s_b(t)$ are accurately recovered.

5. Conclusion

In this work, a new 5D four-wing hyperchaotic system having a flux-controlled memristor model with absolute value function is introduced. Dynamical analysis is performed in terms of equilibrium point, perpetual point, phase portraits, Lyapunov exponents, bifurcations, and spectral entropy. In particular, the phenomenon of extreme multistability with hidden oscillation is revealed and the coexistence of infinite hidden attractors is observed. Then, the 5D multistable FWMHS circuit is designed. Finally, a secure chaotic communication scheme of the 5D multistable FWMHS with disturbance inputs based on parametric modulation theory and Lyapunov stability theory is implemented by a convenient robust high-order sliding mode adaptive controller. The proposed adaptive controller can accurately identify unknown parameters, continuously adjust the gain of the receiver system, and effectively suppress the disturbance inputs of the transmitter and receiver. Numerical simulations are given to demonstrate the validity of the theories and the chaotic secure communication scheme. Our future work is to apply the system to image encryption, random number generator, and other fields.

Data Availability

The data used to support the findings of this study are included within the article.

Conflicts of Interest

The authors declare that they have no conflicts of interest.

Acknowledgments

This work was supported by the National Natural Science Foundation of China under Grant nos. 61504013, 61702052, 61772087, 61674054, and 61801054, Natural Science Foundation of Hunan Province under Grant nos. 2019JJ50648, 2016jj2005, and 2017JJ2049, and Scientific Research Fund of Hunan Provincial Education Department under Grant no. 18A137.

References

[1] J. Jin, L. Zhao, M. Li, Z. Yu, and F. Xi, "Improved zeroing neural networks for finite time solving nonlinear equations," *Neural Computing and Applications*, 2009.

[2] F. Yu, L. Liu, L. Xiao, K. Li, and S. Cai, "A robust and fixed-time zeroing neural dynamics for computing time-variant nonlinear equation using a novel nonlinear activation function," *Neurocomputing*, vol. 350, pp. 108–116, 2019.

[3] L. Zhou, F. Tan, F. Yu, and W. Liu, "Cluster synchronization of two-layer nonlinearly coupled multiplex networks with multi-links and time-delays," *Neurocomputing*, vol. 359, pp. 264–275, 2019.

[4] V.-T. Pham, S. Vaidyanathan, E. Tlelo-Cuautle, and T. Kapitaniak, "Memory circuit elements: complexity, complex systems, and applications," *Complexity*, vol. 2019, p. 4, 2019.

[5] X. Zhang and C. Wang, "A novel multi-attractor period multi-scroll chaotic integrated circuit based on CMOS wide adjustable CCCII," *IEEE Access*, vol. 7, no. 1, pp. 16336–16350, 2019.

[6] J. Jie and L. V. Zhao, "Low voltage low power fully integrated chaos generator," *Journal of Circuits Systems & Computers*, vol. 27, no. 10, Article ID 1850155, 2018.

[7] Q. Yin and C. Wang, "A new chaotic image encryption scheme using breadth-first search and dynamic diffusion," *International Journal of Bifurcation and Chaos*, vol. 28, no. 4, Article ID 1850047, 2018.

[8] Y. Li, C. Wang, and H. Chen, "A hyper-chaos-based image encryption algorithm using pixel-level permutation and bit-level permutation," *Optics and Lasers in Engineering*, vol. 90, pp. 238–246, 2017.

[9] G. Cheng, C. Wang, and H. Chen, "A novel color image encryption algorithm based on hyperchaotic system and permutation-diffusion architecture," *International Journal of Bifurcation and Chaos*, vol. 29, no. 9, Article ID 1950115, 2019.

[10] X. Yang, Q. Zhu, and C. Huang, "Lag stochastic synchronization of chaotic mixed time-delayed neural networks with uncertain parameters or perturbations," *Neurocomputing*, vol. 74, no. 10, pp. 1617–1640, 2017.

[11] B. Vaseghi, M. A. Pourmina, and S. Mobayen, "Finite-time chaos synchronization and its application in wireless sensor networks," *Transactions of the Institute of Measurement and Control*, vol. 40, no. 13, pp. 3788–3799, 2017.

[12] F. Yu, L. Li, B. He et al., "Design and FPGA implementation of a pseudorandom number generator based on a four-wing memristive hyperchaotic system and Bernoulli map," *IEEE Access*, vol. 7, pp. 181884–181898, 2019.

[13] F. Yu, L. Li, Q. Tang, S. Cai, Y. Song, and Q. Xu, "A survey on true random number generators based on chaos," *Discrete Dynamics in Nature and Society*, vol. 2019, Article ID 2545123, 2019.

[14] L. L. Zhou, F. Tan, and F. Yu, "A robust synchronization-based chaotic secure communication scheme with double-layered and multiple hybrid networks," *IEEE Systems Journal*, 2019.

[15] L. Zhou and F. Tan, "A chaotic secure communication scheme based on synchronization of double-layered and multiple complex networks," *Nonlinear Dynamics*, vol. 96, no. 2, pp. 869–883, 2019.

[16] B. Vaseghi, M. A. Pourmina, and S. Mobayen, "Secure communication in wireless sensor networks based on chaos synchronization using adaptive sliding mode control," *Nonlinear Dynamics*, vol. 89, no. 3, pp. 1689–1704, 2017.

[17] X. Zhang, C. Wang, W. Yao, and H. Lin, "Chaotic system with bondorbital attractors," *Nonlinear Dynamics*, vol. 97, no. 4, pp. 2159–2174, 2019.

[18] M. Saleh, C. K. Volos, K. Sezgin, Ü. Çavuşoğlu, and B. Vaseghi, "A chaotic system with infinite number of equilibria located on an exponential curve and its chaos-based engineering application," *International Journal of Bifurcation and Chaos*, vol. 28, no. 9, Article ID 1850112, 2018.

[19] F. Yu, L. Gao, K. Gu, B. Yin, Q. Wan, and Z. Zhou, "A fully qualified four-wing four-dimensional autonomous chaotic system and its synchronization," *Optik*, vol. 131, pp. 79–88, 2017.

[20] C. Volos, J.-O. Maaita, S. Vaidyanathan, V.-T. Pham, I. Stouboulos, and I. Kyprianidis, "A novel four-dimensional hyperchaotic four-wing system with a saddle-focus equilibrium," *IEEE Transactions on Circuits and Systems II: Express Briefs*, vol. 64, no. 3, pp. 339–343, 2017.

[21] F. Yu, C.-H. Wang, J.-W. Yin, and H. Xu, "Novel four-dimensional autonomous chaotic system generating one-, two-, three- and four-wing attractors," *Chinese Physics B*, vol. 20, no. 11, Article ID 110505, 2011.

[22] X. Zhou, C. H. Wang, and X. R. Guo, "A new grid multi-wing chaotic system and its circuit implementation," *Acta Physica Sinica*, vol. 61, no. 20, Article ID 200506, 2012.

[23] L. Zhou, C. Wang, and L. Zhou, "Generating hyperchaotic multi-wing attractor in a 4D memristive circuit," *Nonlinear Dynamics*, vol. 85, no. 4, pp. 2653–2663, 2016.

[24] X. Luo, C. Wang, and Z. Wan, "Grid multi-wing butterfly chaotic attractors generated from a new 3-D quadratic autonomous system," *Nonlinear Analysis: Modelling and Control*, vol. 19, no. 2, pp. 272–285, 2014.

[25] F. Yu, P. Li, K. Gu, and B. Yin, "Research progress of multi-scroll chaotic oscillators based on current-mode devices," *Optik*, vol. 127, no. 13, pp. 5486–5490, 2016.

[26] Q. Deng and C. Wang, "Multi-scroll hidden attractors with two stable equilibrium points," *Chaos: An Interdisciplinary Journal of Nonlinear Science*, vol. 29, no. 9, Article ID 093112, 2019.

[27] X. Zhang and C. Wang, "Multiscroll hyperchaotic system with hidden attractors and its circuit implementation," *International Journal of Bifurcation and Chaos*, vol. 29, no. 9, Article ID 1950117, 2019.

[28] J. Jin, "Programmable multi-direction fully integrated chaotic oscillator," *Microelectronics Journal*, vol. 75, pp. 27–34, 2018.

[29] J. Jin and L. Cui, "Fully integrated memristor and its application on the scroll-controllable hyperchaotic system," *Complexity*, vol. 2019, p. 8, 2019.

[30] F. Yu, L. Liu, B. He et al., "Analysis and FPGA realization of a novel 5D hyperchaotic four-wing memristive system, active control synchronization and secure communication application," *Complexity*, vol. 2019, p. 18, 2019.

[31] V.-T. Pham, S. Vaidyanathan, C. Volos, S. Jafari, and S. T. Kingni, "A no-equilibrium hyperchaotic system with a cubic nonlinear term," *Optik*, vol. 127, no. 6, pp. 3259–3265, 2016.

[32] P. Daltzis, S. Vaidyanathan, V. T. Pham, C. Volos, E. Nistazakis, and G. Tombras, "Hyperchaotic attractor in a novel hyperjerk system with two nonlinearities," *Circuits, Systems, and Signal Processing*, vol. 37, no. 2, pp. 613–635, 2018.

[33] V.-T. Pham, F. Rahma, M. Frasca, and L. Fortuna, "Dynamics and synchronization of a novel hyperchaotic system without equilibrium," *International Journal of Bifurcation and Chaos*, vol. 24, no. 6, Article ID 1450087, 2014.

[34] C. H. Wang, H. Xia, and L. Zhou, "Implementation of a new memristor-based multiscroll hyperchaotic system," *Pramana-Journal of Physics*, vol. 88, no. 2, p. 34, 2017.

[35] H. Lin and C. Wang, "Influences of electromagnetic radiation distribution on chaotic dynamics of a neural network," *Applied Mathematics and Computation*, vol. 369, Article ID 124840, 2020.

[36] C. Wang, L. Xiong, J. Sun, and W. Yao, "Memristor-based neural networks with weight simultaneous perturbation training," *Nonlinear Dynamics*, vol. 95, no. 4, pp. 2893–2906, 2019.

[37] Q. Zhao, C. Wang, and X. Zhang, "A universal emulator for memristor, memcapacitor, and meminductor and its chaotic circuit," *Chaos*, vol. 29, no. 1, Article ID 013141, 2019.

[38] W. Yao, C. Wang, J. Cao, Y. Sun, and C. Zhou, "Hybrid multisynchronization of coupled multistable memristive neural networks with time delays," *Neurocomputing*, vol. 363, pp. 281–294, 2019.

[39] L. Zhou, C. Wang, and L. Zhou, "A novel no-equilibrium hyperchaotic multi-wing system via introducing memristor," *International Journal of Circuit Theory and Applications*, vol. 46, no. 1, pp. 84–98, 2018.

[40] C. Wang, L. Zhou, and R. Wu, "The design and realization of a hyper-chaotic circuit based on a flux-controlled memristor with linear memductance," *Journal of Circuits, Systems and Computers*, vol. 27, no. 3, Article ID 1850038, 2018.

[41] E. Dong, M. Yuan, S. Du, and Z. Chen, "A new class of Hamiltonian conservative chaotic systems with multistability and design of pseudo-random number generator," *Applied Mathematical Modelling*, vol. 73, pp. 40–71, 2019.

[42] V. Sundarapandian, J. Sajad, and V. T. Pham, "A 4-D chaotic hyperjerk system with a hidden attractor, adaptive backstepping control and circuit design," *Archives of Control Sciences*, vol. 28, no. 2, pp. 239–254, 2018.

[43] V.-T. Pham, S. Jafari, C. Volos, and T. Kapitaniak, "Different families of hidden attractors in a new chaotic system with variable equilibrium," *International Journal of Bifurcation and Chaos*, vol. 27, no. 9, Article ID 1750138, 2017.

[44] V.-T. Pham, C. Volos, S. Jafari, and T. Kapitaniak, "A novel cubic-equilibrium chaotic system with coexisting hidden attractors: analysis, and circuit implementation," *Journal of Circuits, Systems and Computers*, vol. 27, no. 4, Article ID 1850066, 2018.

[45] V. T. Pham, C. Volos, S. T. Kingni, T. Kapitaniak, and S. Jafari, "Bistable hidden attractors in a novel chaotic system with hyperbolic sine equilibrium," *Circuits Systems and Signal Processing*, vol. 37, no. 19, pp. 1028–1043, 2017.

[46] V.-T. Pham, X. Wang, S. Jafari, C. Volos, and T. Kapitaniak, "From wang-chen system with only one stable equilibrium to a new chaotic system without equilibrium," *International Journal of Bifurcation and Chaos*, vol. 27, no. 6, Article ID 1750097, 2017.

[47] Z. Wang, H. R. Abdolmohammadi, F. E. Alsaadi, T. Hayat, and V.-T. Pham, "A new oscillator with infinite coexisting asymmetric attractors," *Chaos, Solitons & Fractals*, vol. 110, pp. 252–258, 2018.

[48] V. T. Pham, S. Jafari, C. Volos, and T. Kapitaniak, "A gallery of chaotic systems with an infinite number of equilibrium points," *Chaos, Solitons & Fractals*, vol. 93, pp. 58–63, 2016.

[49] V. T. Pham, S. Jafari, C. Volos, T. Gotthans, X. Wang, and D. V. Hoang, "A chaotic system with rounded square equilibrium and with no-equilibrium," *Optik*, vol. 130, pp. 365–371, 2016.

[50] V.-T. Pham, S. Jafari, X. Wang, and J. Ma, "A chaotic system with different shapes of equilibria," *International Journal of Bifurcation and Chaos*, vol. 26, no. 4, Article ID 1650069, 2016.

[51] L. Zhou, C. Wang, X. Zhang, and W. Yao, "Various attractors, coexisting attractors and antimonotonicity in a simple fourth-order memristive twin-T oscillator," *International Journal of Bifurcation and Chaos*, vol. 28, no. 4, Article ID 1850050, 2018.

[52] B. A. Mezatio, M. T. Motchongom, B. R. Wafo Tekam, R. Kengne, R. Tchitnga, and A. Fomethe, "A novel memristive 6D hyperchaotic autonomous system with hidden extreme multistability," *Chaos, Solitons & Fractals*, vol. 120, pp. 100–115, 2019.

[53] A. Bayani, K. Rajagopal, A. J. M. Khalaf, S. Jafari, G. D. Leutcho, and J. Kengne, "Dynamical analysis of a new multistable chaotic system with hidden attractor: antimonotonicity, coexisting multiple attractors, and offset boosting," *Physics Letters A*, vol. 383, no. 13, pp. 1450–1456, 2019.

[54] K. Xie, X. Ning, X. Wang et al., "An efficient privacy-preserving compressive data gathering scheme in WSNs," *Information Sciences*, vol. 390, no. 2, pp. 702–715, 2016.

[55] K. Gu, W. Jia, G. Wang, and S. Wen, "Efficient and secure attribute-based signature for monotone predicates," *Acta Informatica*, vol. 54, no. 5, pp. 521–541, 2017.

[56] M. Long, F. Peng, and H.-Y. Li, "Separable reversible data hiding and encryption for HEVC video," *Journal of Real-Time Image Processing*, vol. 14, no. 1, pp. 171–182, 2018.

[57] K. Gu, N. Wu, B. Yin, and W. Jia, "Secure data sequence query framework based on multiple fogs," *IEEE Transactions on Emerging Topics in Computing*, 2019.

[58] K. Gu, X. Dong, and L. Wang, "Efficient traceable ring signature scheme without pairings," *Advances in Mathematics of Communications*, 2019.

[59] S. He, W. Zeng, K. Xie et al., "PPNC: privacy preserving scheme for random linear network coding in smart grid," *KSII Transactions on Internet and Information Systems*, vol. 11, pp. 1510–1533, 2017.

[60] Z. Xia, Z. Fang, F. Zou, J. Wang, and A. K. Sangaiah, "Research on defensive strategy of real-time price attack based on multiperson zero-determinant," *Security and Communication Networks*, vol. 2019, p. 13, 2019.

[61] K. Gu, K. M. Wang, and L. Yang, "Traceable attribute-based signature," *Journal of Information Security and Applications*, vol. 49, pp. 1–16, 2019.

[62] M. Long, F. Peng, and Y. Zhu, "Identifying natural images and computer generated graphics based on binary similarity measures of PRNU," *Multimedia Tools and Applications*, vol. 78, pp. 489–506, 2019.
[63] K. Gu, N. Wu, B. Yin, and W. Jia, "Secure data query framework for cloud and fog computing," *IEEE Transactions on Network and Service Management*, 2019.
[64] J.-L. Zhang, W.-Z. Wang, X.-W. Wang, and Z.-H. Xia, "Enhancing security of FPGA-based embedded systems with combinational logic binding," *Journal of Computer Science and Technology*, vol. 32, no. 2, pp. 329–339, 2017.
[65] K. Gu, W. Jia, and C. Jiang, "Efficient identity-based proxy signature in the standard model," *The Computer Journal*, vol. 58, no. 4, pp. 792–807, 2015.
[66] L. Xiang, G. Guo, J. Yu, V. S. Sheng, and P. Yang, "A convolutional neural network-based linguistic steganalysis for synonym substitution steganography," *Mathematical Biosciences and Engineering*, vol. 17, no. 2, pp. 1041–1058, 2020.
[67] Y.-Y. Huang, Y.-H. Wang, and Y. Zhang, "Shape synchronization of drive-response for a class of two-dimensional chaotic systems via continuous controllers," *Nonlinear Dynamics*, vol. 78, no. 4, pp. 2331–2340, 2014.
[68] Y. Huang, Y. Wang, H. Chen, and S. Zhang, "Shape synchronization control for three-dimensional chaotic systems," *Chaos, Solitons & Fractals*, vol. 87, pp. 136–145, 2016.
[69] S. Çiçek, A. Ferikoğlu, and İ. Pehlivan, "A new 3D chaotic system: dynamical analysis, electronic circuit design, active control synchronization and chaotic masking communication application," *Optik*, vol. 127, no. 8, pp. 4024–4030, 2016.
[70] J. M. V. Grzybowski, M. Rafikov, and J. M. Balthazar, "Synchronization of the unified chaotic system and application in secure communication," *Communications in Nonlinear Science and Numerical Simulation*, vol. 14, no. 6, pp. 2793–2806, 2009.
[71] J. He and J. Cai, "Parameter modulation for secure communication via the synchronization of Chen hyperchaotic systems," *Systems Science & Control Engineering*, vol. 2, no. 1, pp. 718–726, 2014.
[72] F. Yu and C. Wang, "Secure communication based on a four-wing chaotic system subject to disturbance inputs," *Optik*, vol. 125, no. 20, pp. 5920–5925, 2014.
[73] J. L. Mata-Machuca, R. Martínez-Guerra, R. Aguilar-López, and C. Aguilar-Ibañez, "A chaotic system in synchronization and secure communications," *Communications in Nonlinear Science and Numerical Simulation*, vol. 17, no. 4, pp. 1706–1713, 2012.
[74] A. Prasad, "Existence of perpetual points in nonlinear dynamical systems and its applications," *International Journal of Bifurcation and Chaos*, vol. 25, no. 2, Article ID 1530005, 2015.
[75] D. Dudkowski, A. Prasad, and T. Kapitaniak, "Perpetual points and hidden attractors in dynamical systems," *Physics Letters A*, vol. 379, no. 40-41, pp. 2591–2596, 2015.
[76] D. Dudkowski, A. Prasad, and T. Kapitaniak, "Describing chaotic attractors: regular and perpetual points," *Chaos*, vol. 28, no. 3, Article ID 033604, 2018.
[77] S. He, K. Sun, and H. Wang, "Complexity analysis and DSP implementation of the fractional-order Lorenz hyperchaotic system," *Entropy*, vol. 17, no. 12, pp. 8299–8311, 2015.
[78] S. He, K. Sun, and S. Banerjee, "Dynamical properties and complexity in fractional-order diffusionless Lorenz system," *European Physical Journal Plus*, vol. 131, p. 254, 2016.
[79] S. He, K. Sun, X. Mei, B. Yan, and S. Xu, "Numerical analysis of fractional-order chaotic system based on conformable fractional-order derivative," *European Physical Journal Plus*, vol. 132, p. 36, 2017.
[80] B. C. Bao, H. Bao, N. Wang, M. Chen, and Q. Xu, "Hidden extreme multistability in memristive hyperchaotic system," *Chaos, Solitons & Fractals*, vol. 94, pp. 102–111, 2017.
[81] S. Laghrouche, F. Plestan, and A. Glumineau, "Higher order sliding mode control based on integral sliding mode," *Automatica*, vol. 43, no. 3, pp. 531–537, 2007.
[82] A. Levant, "Homogeneity approach to high-order sliding mode design," *Automatica*, vol. 41, no. 5, pp. 823–830, 2005.